lubricants

MDPI

Article

Lubrication Performance of Misaligned Journal Bearings with Flexible Structure under Shock Load Conditions

Sung-Ho Hong [1,*] and Woo-Ju Jeon [2]

[1] Department of Mechanical System Engineering, Dongguk University-WISE Campus, Gyeongju-si 38066, Republic of Korea
[2] Department of Mechanical Engineering, Korea Advanced Institute of Science and Technology (KAIST), Daejeon 34141, Republic of Korea; wooju.jeon@samsung.com
* Correspondence: hongsh@dongguk.ac.kr; Tel.: +82-54-770-2211

Abstract: Bearings might be damaged due to shock loads caused by disturbances, in addition to static loads. In this study, a flexible structure was applied to enhance the lubrication characteristics of misaligned journal bearings subjected to impact loads. When an impact load is added to the bearing, a misaligned journal bearing has a high possibility of metal-to-metal contact. It might also lead to failure. Misalignment can occur at any time during bearing operation. A flexible structure is applied to the end of the bearing as a way to improve lubrication performance in a system where impact loads might be applied. The bearing's lubrication performance was numerically assessed under unsteady-state conditions. An elastohydrodynamic lubrication analysis was conducted, taking into account elastic deformation. The lubrication characteristics of misaligned journal bearings were compared with the dimensionless minimum film thickness. The flexible structure and elastic modulus of the bearing were investigated so that it could support the load without contact according to the change in the maximum magnitude of the impact load. When subjected to oil film pressure, this flexible structure underwent elastic deformation, resulting in enlargement of the oil film. A misaligned journal bearing with a suitable flexible structure provided stable lubrication without metal-to-metal contact, even under shock load conditions. The flexible structure was incorporated into the high-load-bearing region of the journal bearing as a groove. Therefore, the application of a flexible structure in misaligned journal bearings can effectively enhance lubrication performance in misaligned conditions and under shock loads.

Keywords: elastohydrodynamic lubrication (EHL); flexible structure; impact load; minimum film thickness; misaligned journal bearing

Citation: Hong, S.-H.; Jeon, W.-J. Lubrication Performance of Misaligned Journal Bearings with Flexible Structure under Shock Load Conditions. *Lubricants* **2023**, *11*, 500. https://doi.org/10.3390/lubricants11120500

Received: 6 September 2023
Revised: 7 November 2023
Accepted: 21 November 2023
Published: 25 November 2023

1. Introduction

Hydrodynamic lubrication generates oil pressure through the relative movement of mating surfaces and creates a lubricant film that completely separates the two contact surfaces [1]. As the shaft rotates, the supporting force from the lubricant film within the bearing and keeps the journal bearing separated [2–4]. However, metal-to-metal contact can occur in journal bearings for various reasons, leading to wear and failure.

Bearings often encounter misalignment of the journal axis, leading to an uneven distribution of film thickness for bearing clearance along the axial direction. This irregular distribution is primarily caused by factors such as asymmetric loads and errors during installation [5–7]. In addition, during operation, a bearing is bound to encounter diverse forms of disturbances arising from shock loads. The impact of these shock loads will inevitably influence both the bearing's performance during operation and its overall service life [8]. Moreover, shock can induce rapid and early failure of high-speed bearings [9,10].

Even a minor misalignment angle between shafts and bearings resulting from manufacturing errors, non-central loads or shaft deformation can change the distribution of the oil film. As a consequence of this misalignment, the oil film pressure, load carrying capacity

and frictional force of the bearing undergo considerable variations [11,12]. Furthermore, inadequate operational quality can induce undesirable shaft vibrations [13].

Related studies can be largely divided into numerical studies, experimental studies [14] and studies [15–17] that combine numerical and experimental research. Most of them are numerical studies that perform CFD (computational fluid dynamics) analysis based on the FSI (fluid–structure interaction) technique [18], THD (thermohydrodynamic) analysis [19–21], EHD (elastohydrodynamic) analysis [22,23] and TEHD (thermoelastohydrodynamic) analysis [5,24]. Various methods have been proposed to enhance the lubrication performance of misaligned journal bearings. In terms of bearing material, a ZA-27 alloy [25] and a carbon-fiber phenolic composite [26] can be applied to improve the lubrication characteristics. To improve the lubrication characteristics, micropolar fluid [7] can be applied as lubricant in terms of lubricant, and a profile [7,27] or flexible structure [23,28–30] can be applied in terms of design. The grooved area experiences elastic deformation as a result of the oil film pressure exerted on the surface of the journal bearing. This can increase oil film thickness, effectively avoiding direct metal contact resulting from misalignment of the bearing. In a static load condition, when the groove is applied to the end of journal bearing, a larger oil film can be obtained in terms of the minimum film thickness than when the groove is not applied. However, when grooves of inappropriate geometries are applied, the minimum oil film thickness is smaller than when grooves are not applied [23]. Thus, to improve the lubricating properties of misaligned journal bearings under static load conditions, it is necessary to apply an appropriate flexible structure according to the operating conditions.

Several studies have been conducted on the shock behavior of different types of bearings, including oil bearings [31–34], air bearings [35,36] and water-lubricated bearings [37]. One study found that as the amplitude of random shock load increases, the average service life of sliding bearings decreases [31]. Another investigation revealed that rotor stability and vibration amplitude were favorable when foil bearings supported the rotor under various test conditions [35]. Furthermore, it has been reported that the use of double bladder structures can enhance the stability of water-lubricated bearings when subjected to half-sine shock load [37]. A study was conducted using a chamfer and profile to improve the lubrication characteristics of misaligned journal bearings under conditions where no shock load was applied [38] Moreover, lobe-type profiles or pockets were applied to the bearings to improve the lubrication characteristics under impact load conditions [37–40]. A study was conducted using a chamfer and profile to improve the lubrication characteristics of misaligned journal bearings under conditions where no shock load was applied [41–43].

The chamfer and profile were applied to minimize the vibration amplitude and to enhance the turbine stability limits. Research is also being conducted on methods to appropriately describe impact loads [44–46].

Some studies have been conducted to improve the lubrication characteristics of misaligned journal bearings. There are also studies on the lubrication characteristics of bearings against impact loads. However, studies applying a flexible structure when an impact load is applied to a misaligned journal bearing for improving lubrication characteristics have not been reported yet. Moreover, there are few analyses conducted under large-impact-load conditions. Thus, the objective of this study was to evaluate the lubrication performance of a groove-type flexible structure for preventing metal-to-metal contact under large-shock-load conditions, where the maximum value of the impact load was approximately three times the static load. In addition, the effect of an elastic modulus according to impact load condition within the range of the elastic modulus of bearing steel was evaluated. A numerical study was conducted on the design of an appropriate flexible structure that could prevent metal-to-metal contact under the shock load condition of misaligned journal bearings.

2. Numerical Model and Method

EHL analysis was performed to estimate the lubrication performance of the misaligned journal bearing under the given condition of an impact load. A flexible structure was applied to prevent metal-to-metal contact due to impact. EHL analysis was performed to consider elastic deformation due to oil film pressure. In this research, lubrication performance was evaluated over time using commercial software, COMSOL Version 6.0, capable of multi-physics analysis. This analysis software is based on the finite element method. It discretizes non-linear governing equations into algebraic equations. The numerical analysis involved the utilization of three key modules. The first module, known as the hydrodynamic bearing module, was utilized to analyze hydrodynamic lubrication. The second module, the solid mechanics module, was employed to study the elastic deformation of the bearing. Finally, the third module, called the solid–bearing coupling module, enabled smooth integration and interaction between the hydrodynamic bearing and solid mechanics modules [23]. The hydrodynamics bearing formula and the solid mechanics formula were combined into one matrix, and the calculation was performed using a fully coupled method. The linear elastic material model was applied to the flexible area (groove) where deformation occurs, and the rigid material model was applied to other parts. The geometric part to which the rigid body model was applied was given the condition of being fully constrained (deformation = 0). A rigid material model was applied to the rotation axis, and full constraints were applied in the axial direction (*z*-axis).

Misaligned journal bearings can lead to metal-to-metal contact at the end of the bearing due to various causes, as shown in Figure 1a. To prevent contact between metals, a flexible structure was applied, as represented by the black dotted line in Figure 1b. The flexible structure had a ring-type groove that could secure larger oil film thickness through elastic deformation caused by oil film pressure at the end of the bearing.

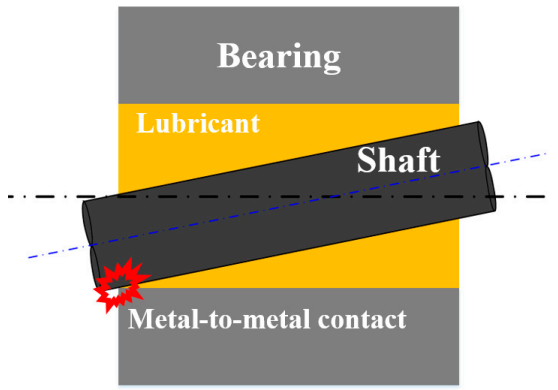

(**a**)

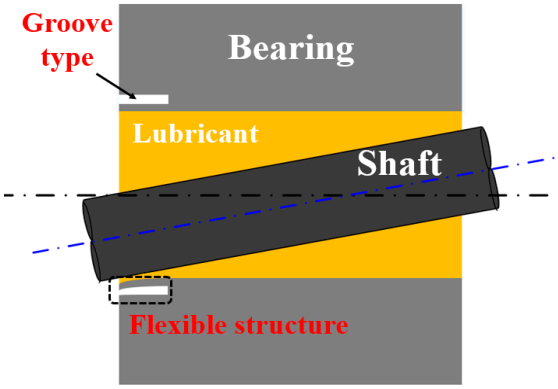

(**b**)

Figure 1. Misaligned journal bearing: (**a**) metal-to-metal contact; (**b**) application of a flexible structure.

Figure 2 presents a schematic of a journal bearing with a flexible structure. The rigid shaft rotates about the z-axis with an angular velocity ω. To the center of the shaft, at $z = l/2$, a load w is exerted in the direction of θ_w. The flexible structure is located in the dotted regions of Figure 2b. It is applied at the end of the bearing using a groove to induce elastic deformation. The dimensions of the flexible structure are determined by its inner end thickness (d), outer end thickness (a) and length (l_f). The shape of the flexible structure in the axial direction is determined by γ ($=d/a$), which can result in either a rectangular (for $\gamma = 1$) or a tapered (for $\gamma > 1$) shape, as shown in Figure 2c. In a previous analysis of the static load condition, lubrication performance was better when the groove shape was rectangular than when it was tapered [23]. Based on previous results, only cases where the shape of the groove was rectangular were considered in this study. The non-grooved section of the bearing surface remains rigid due to its large thickness, preventing any elastic deformation. The configurations of the journal bearing and the flexible structure are depicted by dimensionless parameters, as specified in Equation (1):

$$A = \frac{a}{r},\ L = \frac{l}{r},\ L_f = \frac{l_f}{l},\ \beta = \frac{c}{r},\ \gamma = \frac{d}{a} \tag{1}$$

The Reynolds equation is employed to solve the oil film pressure (p) under unsteady-state conditions, as demonstrated in Equation (2):

$$\frac{1}{r^2}\frac{\partial}{\partial\theta}\left(h^3\frac{\partial p}{\partial\theta}\right) + \frac{\partial}{\partial z}\left(h^3\frac{\partial p}{\partial z}\right) = 6\eta\omega\frac{\partial h}{\partial\theta} + 12\eta\frac{\partial h}{\partial t} \tag{2}$$

The dimensionless form of equation (2) becomes:

$$\frac{\partial}{\partial\theta}\left(H^3\frac{\partial P}{\partial\theta}\right) + \frac{\partial}{\partial Z}\left(H^3\frac{\partial P}{\partial Z}\right) = \frac{\partial H}{\partial\theta} + 2\frac{\partial H}{\partial T} \tag{3}$$

where p_a is the atmospheric pressure, and the dimensionless variables are:

$$H = \frac{h}{c},\ P = \frac{c^2(p - p_a)}{6r^2\eta\omega},\ X = \frac{x}{r},\ Y = \frac{y}{r},\ Z = \frac{z}{r},\ T = \omega t \tag{4}$$

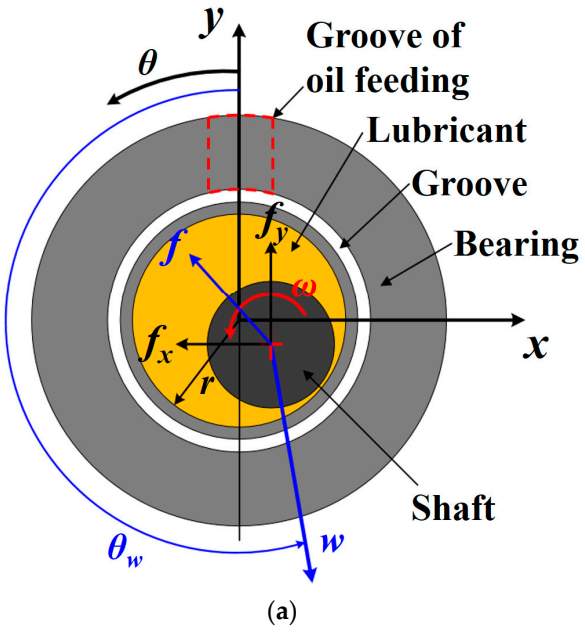

(**a**)

Figure 2. *Cont.*

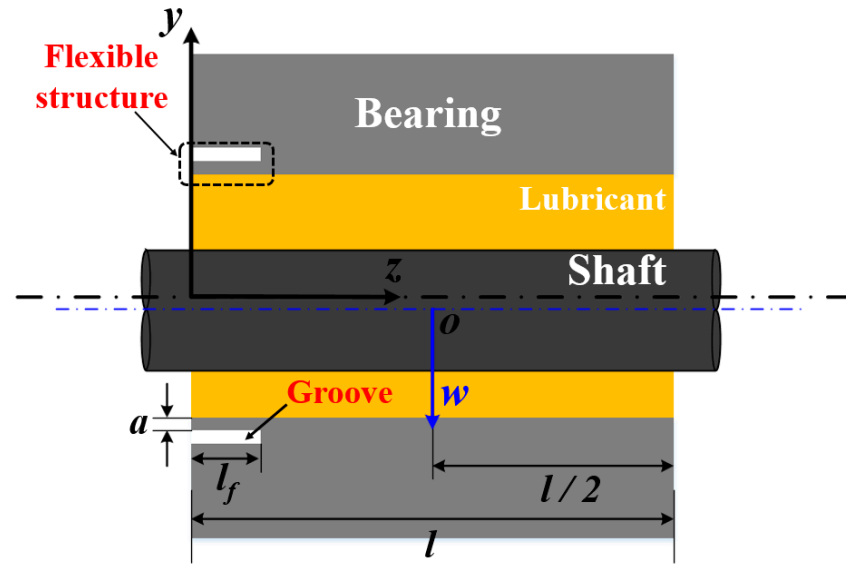

(**b**)

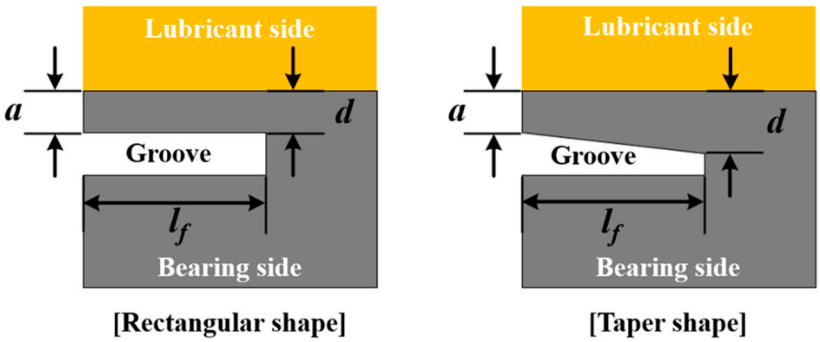

(**c**)

Figure 2. Schematic of journal bearing with flexible structure: (**a**) *x*-*y* plane; (**b**) *y*-*z* plane; (**c**) shapes of the flexible structure.

To determine the oil film pressure in Equation (2), it is essential to determine the oil film thickness (h) in the space between the bearing and shaft. Figure 3 illustrates the shaft's motion, which involves eccentric and tilted movements. The midpoint of the shaft at the location where z equals $l/2$ is designated as O, while O_1 and O_2 represent the midpoints of the shaft at the ends of the bearing. In Figure 3a, two circles depict cross-sections of the shaft projected onto the *x*-*y* plane, with O_1 and O_2 serving as their centers. The eccentricity e represents the distance on the *x*-*y* plane between the center of the bearing and O. The angle ψ on the *x*-*y* plane indicates the altitude angle between the direction of the load and the straight line passing through O and the center of the bearing. The tilting orientation of the shaft aligns with θ_w, and the tilting amount e' is equivalent to half the distance between O_1 and O_2 on the *x*-*y* plane.

Under the aligned condition with zero tilt, the shaft rotates within the bearing. The thickness of the oil film between the shaft and bearing is computed using Equation (5) [23].

$$h = c + e \cdot cos\{\theta - (\theta_W - \pi + \psi)\} + e'\left(1 - \frac{2}{l}z\right)cos\{\theta - (\theta_W - \pi)\} + h_e \quad (5)$$

The non-dimensionalized representation of Equation (5) can be expressed as follows:

$$H = 1 + \varepsilon \cdot cos\{\theta - (\theta_W - \pi + \psi)\} + \varepsilon'\left(1 - 2\frac{Z}{L}\right)cos\{\theta - (\theta_W - \pi)\} + H_e \quad (6)$$

where

$$H_e = \frac{h_e}{c},\ \varepsilon = \frac{e}{c},\ \varepsilon' = \frac{e'}{c} \tag{7}$$

The parameters ε and ε' featured in Equation (7) represent the shaft's eccentricity and tilting ratios, respectively. Additionally, in order to calculate Equation (5), obtaining the alteration in oil film thickness due to the elastic deformation of the flexible structure, denoted as h_e, is essential. The assessment of the elastic deformation of the bearing is conducted through the solid mechanics module. The obtained numerical results are integrated with the hydrodynamic bearing module for hydrodynamic lubrication analysis. Figure 4 displays a hexahedral mesh of the finite element model [23]. The preference for a hexahedral mesh in numerical calculations arises from its superior resolution and faster processing speed compared to the tetrahedral mesh [47]. In the analysis, 100 elements were utilized in the circumferential direction and 53 elements in the axial direction, with the exception of the groove region, where 108 elements were used in the circumferential direction. As a result, the total element count was 44,425.

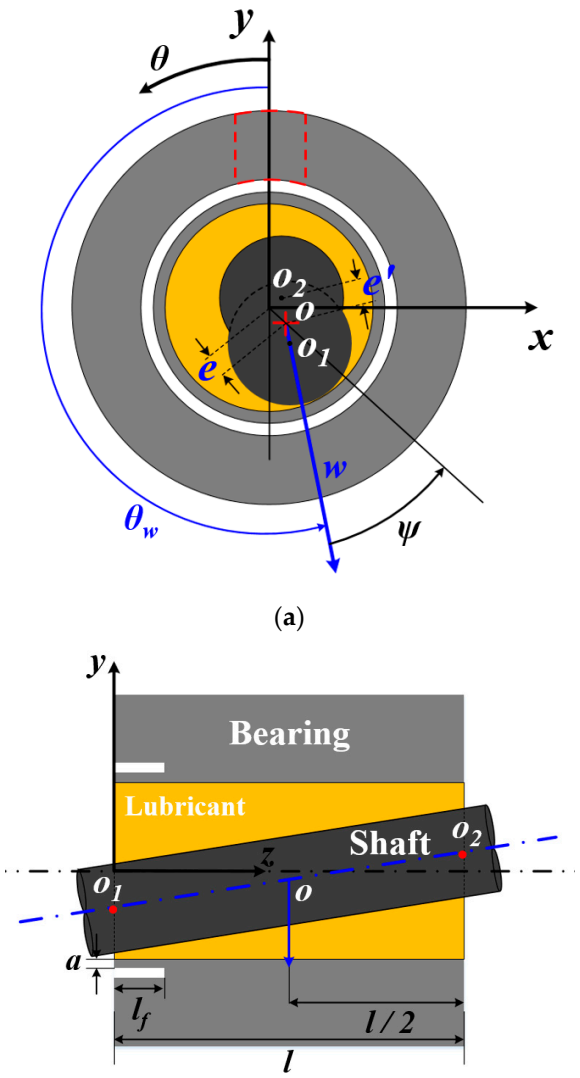

Figure 3. The shaft in the bearing under eccentric and tilted motion conditions: (**a**) *x*-*y* plane; (**b**) *y*-*z* plane.

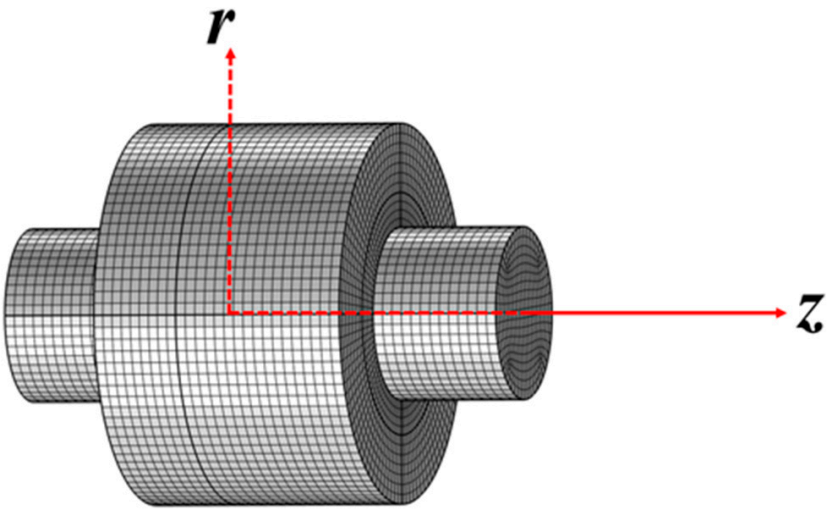

Figure 4. Finite element model of journal bearing.

The boundary conditions for solving Equations (2) and (8) are specified as follows:

- Boundary condition for the oil film fracture zone: $\frac{\partial p}{\partial n} = 0,\ p = p_a$.
- Pressure in the cavitation region:

$$p = p_a \ \text{ where } \ p < p_a. \tag{8}$$

- Pressure at the bearing ends and oil feeding groove $p(0,\ z) = p_b,\ p(\theta,\ 0) = p_b,\ p(\theta,\ l) = p_b$.
- Displacement at the inner end of the flexible structure: $u\left(x,\ y,\ l_f\right) = 0$.

The direction of vector n, as indicated in Equation (8), is perpendicular to the boundary line of the oil film fracture. Additionally, periodic conditions are applied for both pressure and displacement in the ring-shaped bearing. Equation (8) can be expressed in a dimensionless form, given by Equation (9) [23]:

- Boundary condition for the oil film fracture zone: $\frac{\partial P}{\partial n} = 0,\ P = 0$.
- Pressure in the cavitation region:

$$P = 0 \ \text{ where } \ P < 0. \tag{9}$$

- Pressure at the oil feeding groove and the bearing ends:

$$P(0,\ Z) = P_b,\ P(\theta,\ 0) = P_b,\ P(\theta,\ L) = P_b.$$

- Deformation at the inner end of the flexible structure: $U\left(X,\ Y,\ L_f\right) = 0$.

The oil film force, represented as f_o, arises from the oil film pressure. It is utilized to determine the shaft's motion through comparison with the applied load. Figure 2a illustrates the visualization of the oil film force exerted on the shaft. The components of the oil film force in the x and y directions, denoted as f_{ox} and f_{oy}, respectively, were computed using Equations (10) and (11). The calculation of the oil film force was achieved through Equation (12) [23]:

$$f_{ox} = \int_0^l \int_0^{2\pi} p\ r\ sin\theta d\theta dz \tag{10}$$

$$f_{oy} = -\int_0^l \int_0^{2\pi} p\ r\ cos\theta d\theta dz \tag{11}$$

$$f_o = \sqrt{{f_{ox}}^2 + {f_{oy}}^2} \tag{12}$$

Equations (13)–(15) are dimensionless forms of Equations (10)–(12).

$$F_{OX} = \int_0^L \int_0^{2\pi} P\, sin\theta d\theta dz \tag{13}$$

$$F_{OY} = -\int_0^L \int_0^{2\pi} P\, cos\theta d\theta dz \tag{14}$$

$$F_O = \sqrt{F_{OX}{}^2 + F_{OY}{}^2} \tag{15}$$

$$F_{OX} = \frac{c^2 f_{ox}}{6r^4 \eta\omega},\ F_{OY} = \frac{c^2 f_{oy}}{6r^4 \eta\omega},\ F_O = \frac{c^2 f_o}{6r^4 \eta\omega} \tag{16}$$

The load used in the analysis is shown in Figure 5. The analysis was performed under the condition that the impact load was added to the static load. In Figure 5, T_1 and T_3 are time intervals in which only the dimensionless static load W acts. T_2 is the time interval in which the impact load acts together with the static load. The impact load is assumed to be in the form of a wave with attenuation. The analysis was performed for cases where the maximum value of the total load given was 1.5 times (W_{max} = 1.5 W), 2 times (W_{max} = 2 W) or 3 times (W_{max} = 3 W) the static load. In the case of actual misaligned journal bearings, shocks and impulses are applied in various directions in addition to the vertical load. In this study, in order to evaluate the lubrication characteristics of the flexible structure under impact load conditions, it was simply assumed that the impact load acts in the vertical direction.

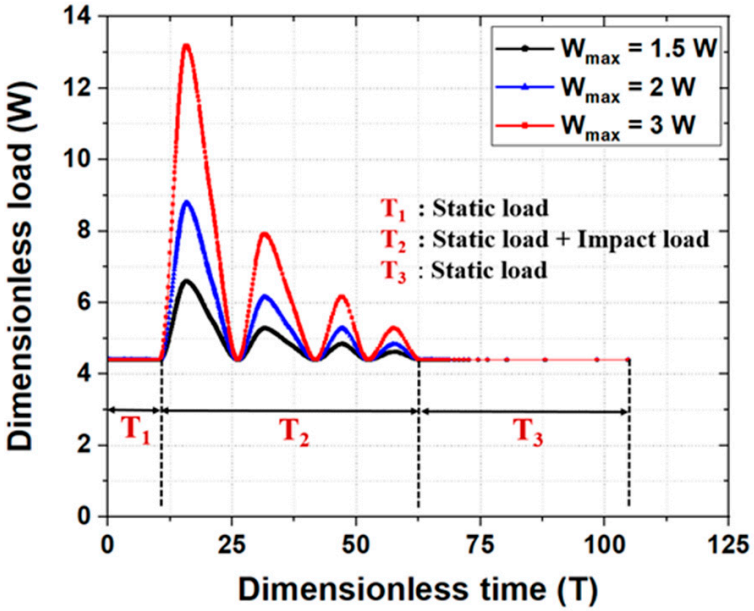

Figure 5. Dimensionless load conditions with dimensionless time.

The dynamic viscosity and density of the lubricant used in the analysis were 0.02083 Pa·s and 904 kg/m^3, respectively. It is difficult to specify information about the actual size and lubricant due to company security reasons since this is an interpretation of journal bearings applied to the home appliances of electronic company. Therefore, a dimensionless analysis was performed.

3. Numerical Results and Discussion

In a previous study [23], EHL analysis [48–53] was performed for a misaligned journal bearing with a flexible structure under a static load condition. The flexible structure of the misaligned journal bearing effectively increased the minimum film thickness. This was because the oil film thickness increased via elastic deformation in the flexible structure at the end of the bearing, with the lubrication performance of the bearings improved, as shown in Figure 6. From the overall dimensionless displacement in Figure 6, it can be confirmed that there is appropriate deformation due to oil film pressure in the area where the flexible structure was applied. In addition, a rectangular-shaped flexible structure was more effective in improving lubrication characteristics than a taper-shaped one [23]. Therefore, in this study, lubrication characteristics under impact load conditions were evaluated for misaligned journal bearings to which a rectangular-shaped flexible structure was applied. In addition, when metal-to-metal contact occurred in misaligned journal bearings, the elastic modulus of the bearing steel was changed, and the lubrication characteristics were compared with those of the existing bearing steel.

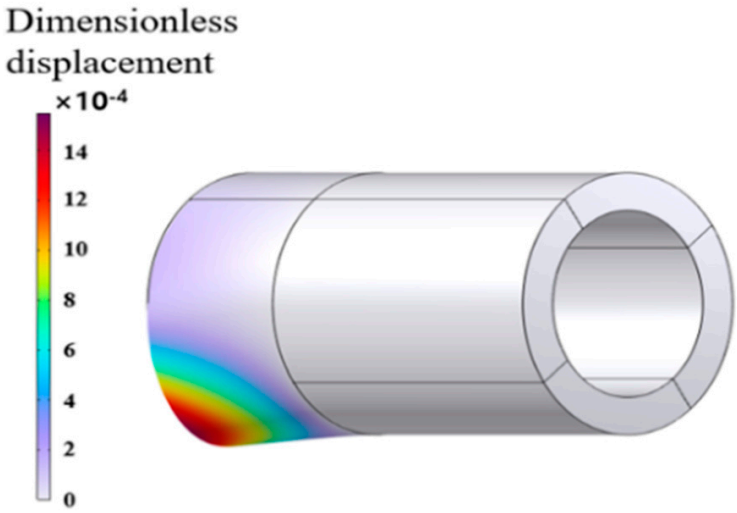

Figure 6. Dimensionless displacement of overall misalignment journal with flexible structure.

The lubrication characteristics following a change in the flexible structure geometry and a change in the tilting ratio (ε') were examined under three load conditions in which the impact load and the static load acted together. Changes in the dimensionless thickness (A) and length (L_f) were used to vary the geometry of the flexible structure. The dimensionless thickness ratio (γ) of the flexible structure was constant at 1 because it was found that the flexible structure with a rectangular shape was more effective than the taper-shaped one in improving the lubrication characteristics [23].

The dimensionless minimum oil film thickness due to changes in the dimensionless thickness (A) of the flexible structure was investigated over time, as shown in Figure 7. The lubrication characteristics were compared under three load conditions and two elastic modulus conditions with other specifications, as shown in Table 1. When A was increased, the dimensionless minimum film thickness decreased overall, resulting in poor lubrication characteristics. When A was 0.6 and 0.8, the difference in the dimensionless minimum oil film thickness was very small. However, when A exceeded 0.8, the advantage of the flexible structure did not appear under impact load conditions. This was because when A exceeded a certain value, the elastic deformation due to oil film pressure was rapidly reduced. In other words, when A exceeded a certain value, it was difficult to secure sufficient oil film thickness through elastic deformation. As the maximum load due to impact load increased, the lubrication properties deteriorated. Additionally, when the dimensionless elastic modulus (E^*) was reduced by about 32% to 1.5×10^4, the overall lubrication characteristics were improved.

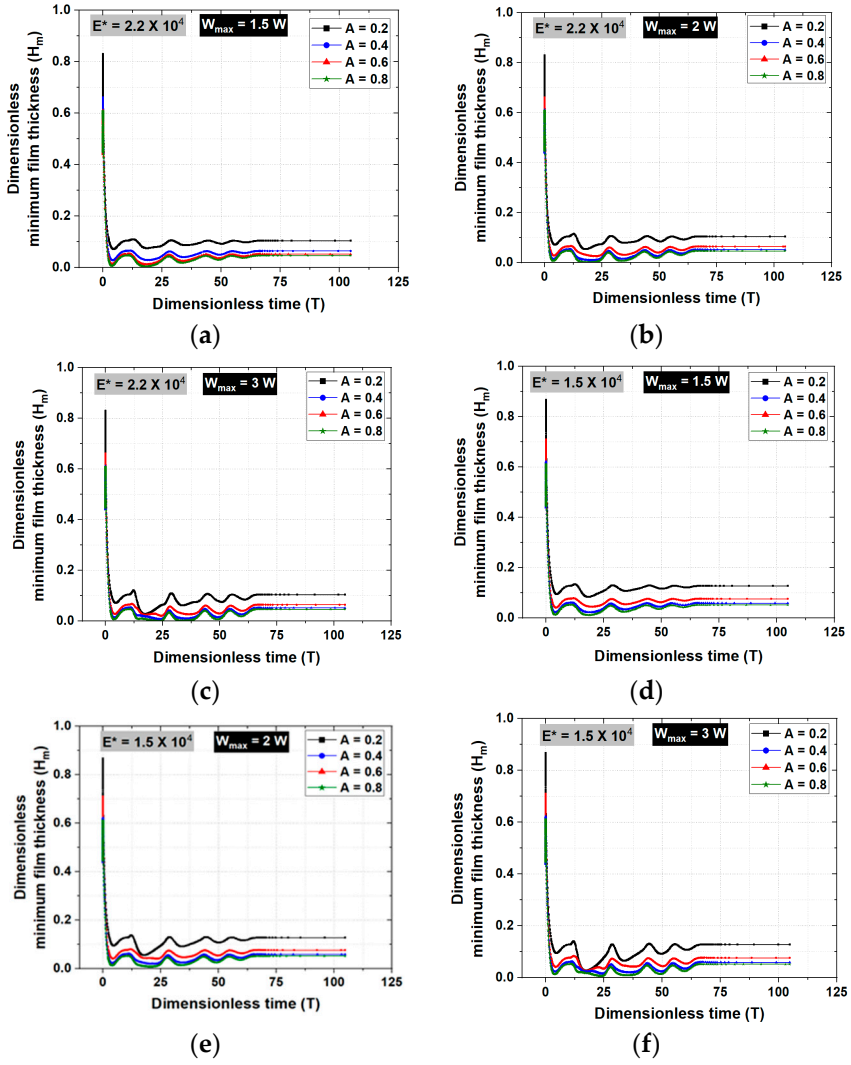

Figure 7. Dimensionless minimum film thickness with A: (**a**) $E^* = 2.2 \times 10^4$, $W_{max} = 1.5\ W$; (**b**) $E^* = 2.2 \times 10^4$, $W_{max} = 2\ W$; (**c**) $E^* = 2.2 \times 10^4$, $W_{max} = 3\ W$; (**d**) $E^* = 1.5 \times 10^4$, $W_{max} = 1.5\ W$; (**e**) $E^* = 1.5 \times 10^4$, $W_{max} = 2\ W$; (**f**) $E^* = 1.5 \times 10^4$, $W_{max} = 3\ W$.

Table 1. Specification of the analysis model (variation in A, W and E^*).

Parameter	Value	Parameter	Value
A	0.2, 0.4, 0.6, 0.8	W	$W_{max} = 1.5\ W$, $2\ W$, $3\ W$
E^*	2.2×10^4, 1.5×10^4	β	10^{-3}
L	3.0	γ	1.0
L_f	1/3	ε'	0.2
P_b	0.3		

The smallest dimensionless minimum film thickness within the dimensionless time region of Figure 7 is shown in Figure 8. In the analysis results under static load conditions, the lubrication characteristics were good even when A was 1.4. It is almost unrealistic to apply conditions where A is 0.8 or more. The actual applicable range will be 0.4 or less. However, this analysis was performed to show that the lubrication characteristics were improved by the flexible structure even when the total load was about three times the static load.

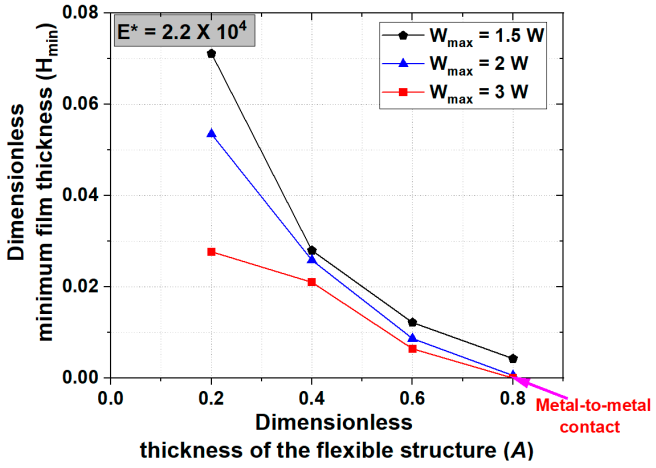

(**a**)

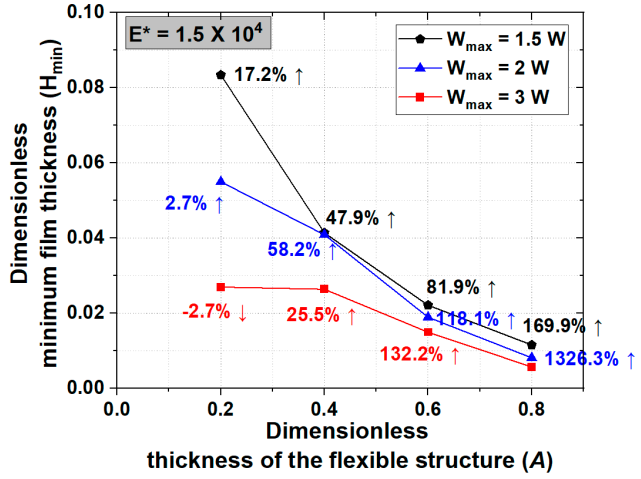

(**b**)

Figure 8. Dimensionless minimum film thickness with A and W_{max}: (**a**) $E^* = 2.2 \times 10^4$; (**b**) $E^* = 1.5 \times 10^4$.

The analysis was performed to show that the lubrication characteristics were improved by the flexible structure even when the total load was about three times the static load. However, as shown in Figure 8a, when the maximum load was 3 times and A was 0.8 times the static load, metal-to-metal contact occurred. Similar to the results shown in Figure 7, it was confirmed that when A was increased, the dimensionless minimum film thickness decreased. Moreover, when A was 0.8, metal-to-metal contact did not occur when the maximum load was 1.5 and 2 times the static load. However, they had a very small dimensionless minimum film thickness, leading to poor lubrication characteristics. To prevent contact between metals, the lubrication characteristics were investigated by changing the dimensionless elastic modulus of the bearing. By reducing the elastic modulus, deformation due to oil film pressure was made easier in the flexible structure. Figure 8a,b show the results when the dimensionless elastic modulus was 2.2×10^4 and 1.5×10^4, respectively. When the dimensionless elastic modulus is reduced by about 32%, the change in lubrication characteristics is expressed as a percentage, as shown Figure 8b. The percentage is expressed as a percentage of the difference in the dimensionless minimum film thickness at the two elastic moduli based on the dimensionless minimum film thickness in the case of the existing dimensionless elastic modulus ($E^* = 2.2 \times 10^4$). The lubrication characteristics were generally improved when the dimensionless elastic modulus was 1.5×10^4. In particular, looking at the case where A was 0.8, when contact occurred or the dimensionless minimum oil film thickness was very small, it was confirmed that no contact occurred and the lubrication characteristics were greatly improved. Figure 9 shows the

dimensionless minimum film thickness and dimensionless maximum displacement with variation in the dimensionless time for four cases among the results in Figure 8. The point when the dimensionless minimum film thickness was the smallest is indicated by a blue dotted line. The point when the maximum dimensionless displacement was the greatest is indicated by a red dotted line. When the dimensionless elastic modulus was 2.2×10^4 and A was 0.2, the point when the dimensionless minimum film thickness was the smallest and the point when the dimensionless maximum displacement was the greatest were almost similar in the entire dimensionless time region. However, when A was 0.6, these two points in dimensionless time, when the dimensionless minimum oil film thickness was the smallest and when the dimensionless maximum deformation was the greatest, were clearly different. This pattern of results was similar even when the dimensionless elastic modulus was 1.5×10^4. Depending on the change in A, the results varied depending on the reactivity of the flexible structure. In other words, when A was small, the deformation of the flexible structure was immediate due to the oil film pressure. However, when A was large, it was believed that the influence of the deformation in the flexible structure had a slight delay. Figures 10 and 11 show dimensionless film thickness distribution and oil pressure distribution, respectively, at the point where the smallest dimensionless minimum film thickness occurs in the time region. At this time, A was 0.4, the maximum load was 1.5 times, 2 times and 3 times the static load, and the dimensionless elastic moduli were 2.2×10^4 and 1.5×10^4. Figure 10 shows a similar pattern of dimensionless film thickness distribution. However, in Figure 10f, where the maximum load was 3 times the static load and the dimensionless elastic modulus was small, at 1.5×10^4, it shows a different form. In this case, the regions where the dimensionless film thickness is large and small are relatively large. That is, under conditions where the dimensionless elastic modulus is small and the maximum load is large, the hydrodynamic pressure increases, and elastic deformation due to the generated oil film pressure is easy. In Figure 11, under the condition that the non-dimensional elastic modulus was the same, when the maximum load is increased, the hydrodynamic oil pressure in the area where oil film pressure occurred is relatively increased.

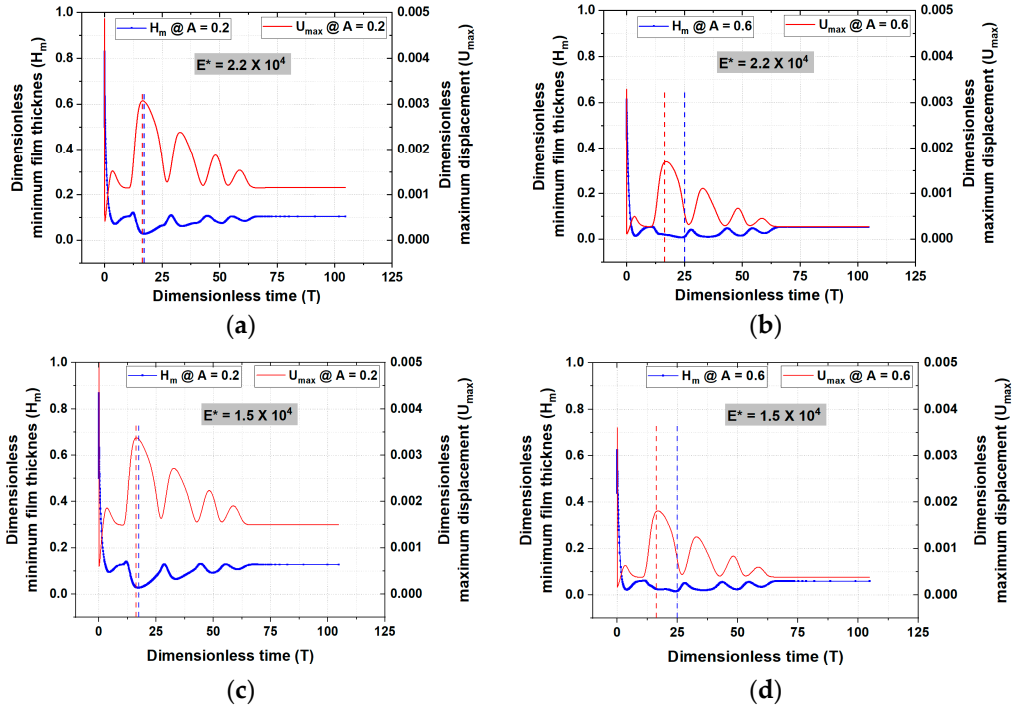

Figure 9. Relationship between dimensionless minimum film thickness and dimensionless maximum displacement with variation in dimensionless time: (**a**) $A = 0.2$, $E^* = 2.2 \times 10^4$; (**b**) $A = 0.6$, $E^* = 2.2 \times 10^4$; (**c**) $A = 0.2$, $E^* = 1.5 \times 10^4$; (**d**) $A = 0.6$, $E^* = 1.5 \times 10^4$.

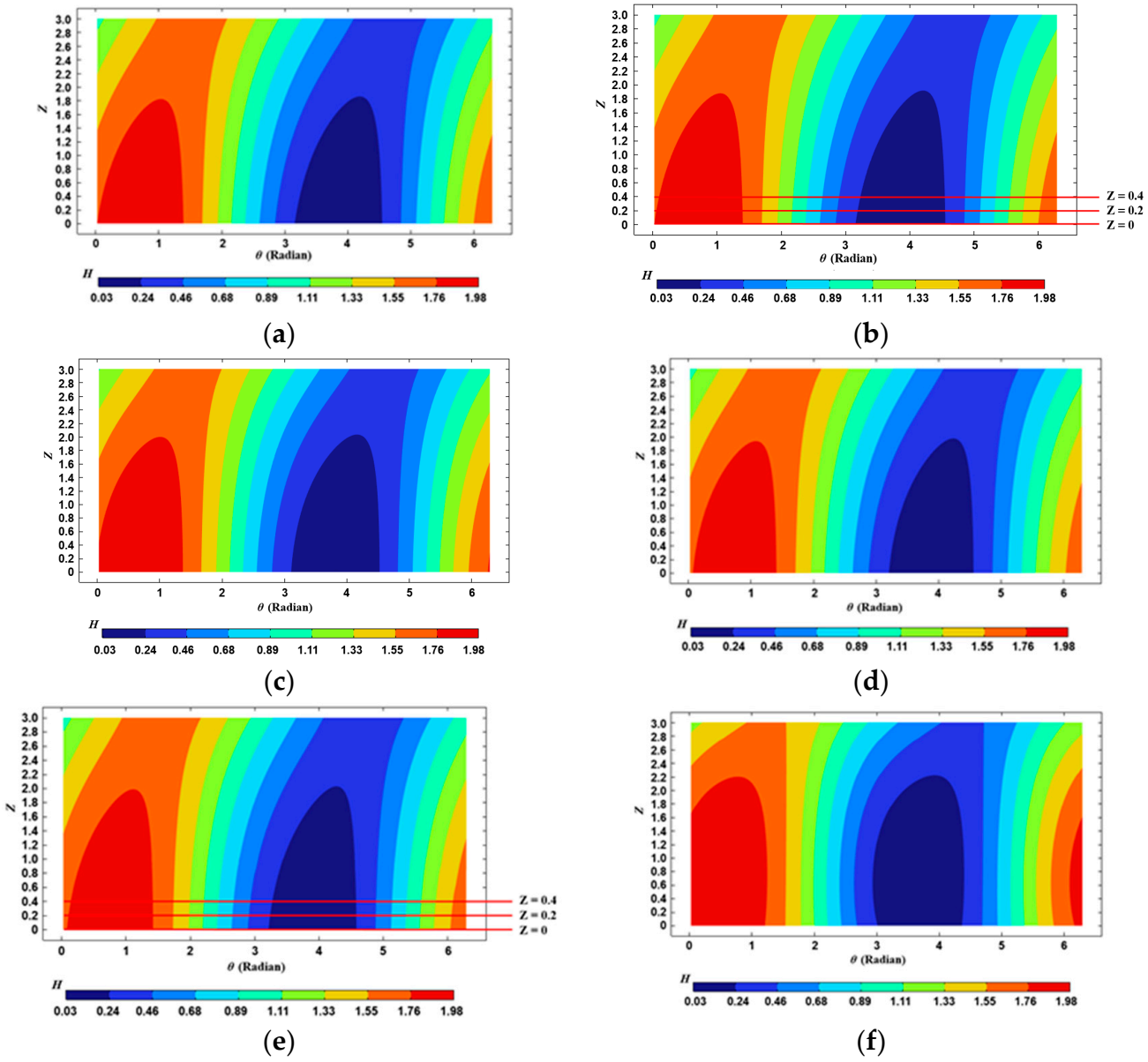

Figure 10. Dimensionless film thickness distribution with E^* and W_{max}: (**a**) $E^* = 2.2 \times 10^4$, $W_{max} = 1.5\ W$; (**b**) $E^* = 2.2 \times 10^4$, $W_{max} = 2\ W$; (**c**) $E^* = 2.2 \times 10^4$, $W_{max} = 3\ W$; (**d**) $E^* = 1.5 \times 10^4$, $W_{max} = 1.5\ W$; (**e**) $E^* = 1.5 \times 10^4$, $W_{max} = 2\ W$; (**f**) $E^* = 1.5 \times 10^4$, $W_{max} = 3\ W$.

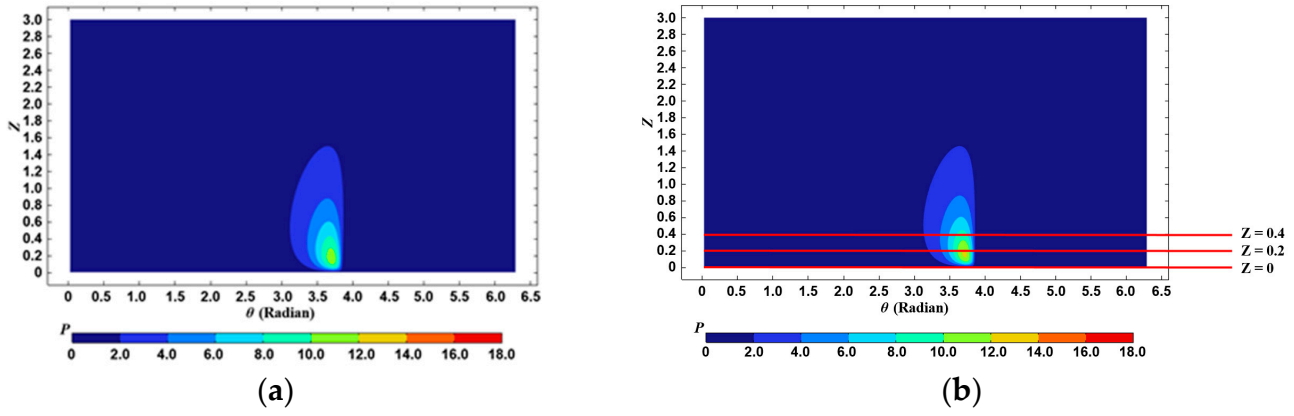

Figure 11. *Cont.*

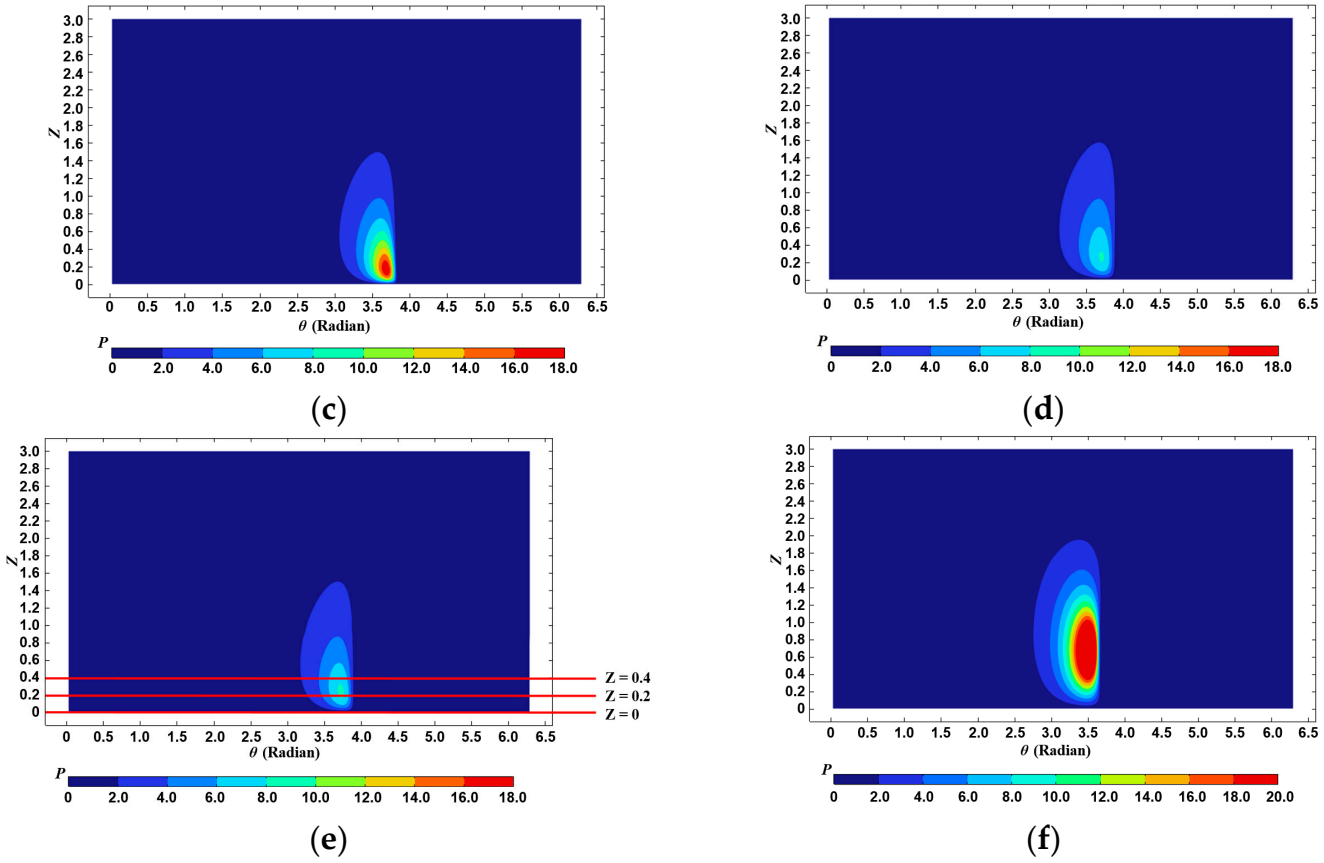

Figure 11. Dimensionless pressure distribution with E^* and W_{max}: (**a**) $E^* = 2.2 \times 10^4$, $W_{max} = 1.5\ W$; (**b**) $E^* = 2.2 \times 10^4$, $W_{max} = 2\ W$; (**c**) $E^* = 2.2 \times 10^4$, $W_{max} = 3\ W$; (**d**) $E^* = 1.5 \times 10^4$, $W_{max} = 1.5\ W$; (**e**) $E^* = 1.5 \times 10^4$, $W_{max} = 2\ W$; (**f**) $E^* = 1.5 \times 10^4$, $W_{max} = 3\ W$.

Figure 12 shows the dimensionless film thickness and dimensionless pressure in the circumferential direction for the three red lines shown in Figures 10b,e and 11b,e. Figure 12a,b show the results when the maximum load is twice the static load and the dimensionless elastic moduli are 2.2×10^4 and 1.5×10^4, respectively. Compared to the static load analysis results [23], it was found that the location where the maximum load occurred moved toward the edge of the bearing. Moreover, after the dimensionless maximum pressure occurred, a dimensionless minimum film thickness occurred, that is, the two points mentioned above did not coincide. The displacement distribution was investigated at the point where the minimum film thickness occurred. Figure 13 shows the dimensionless displacement at the point where the smallest dimensionless minimum film thickness occurs in the time region. At this time, A was 0.4, the maximum load was 1.5 times, 2 times and 3 times the static load, and the dimensionless elastic modulus was 2.2×10^4 or 1.5×10^4. As the dimensionless maximum load increased, the area where deformation occurred widened, with its size increasing overall. Moreover, when the dimensionless elastic modulus was small, more deformation occurred. In other words, the lubrication characteristics were improved as the oil film thickness was relatively large due to a larger amount of elastic deformation.

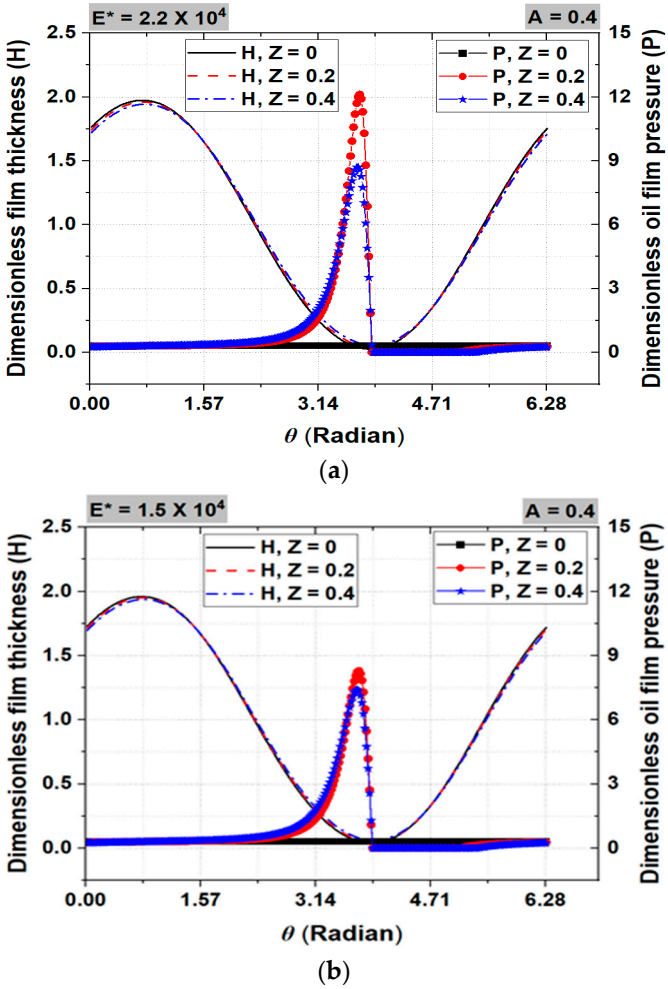

Figure 12. Circumferential distribution of dimensionless film thickness and pressure: (**a**) $A = 0.4$, $W_{max} = 2\ W$, $E^* = 2.2 \times 10^4$; (**b**) $A = 0.4$, $W_{max} = 2\ W$, $E^* = 1.5 \times 10^4$.

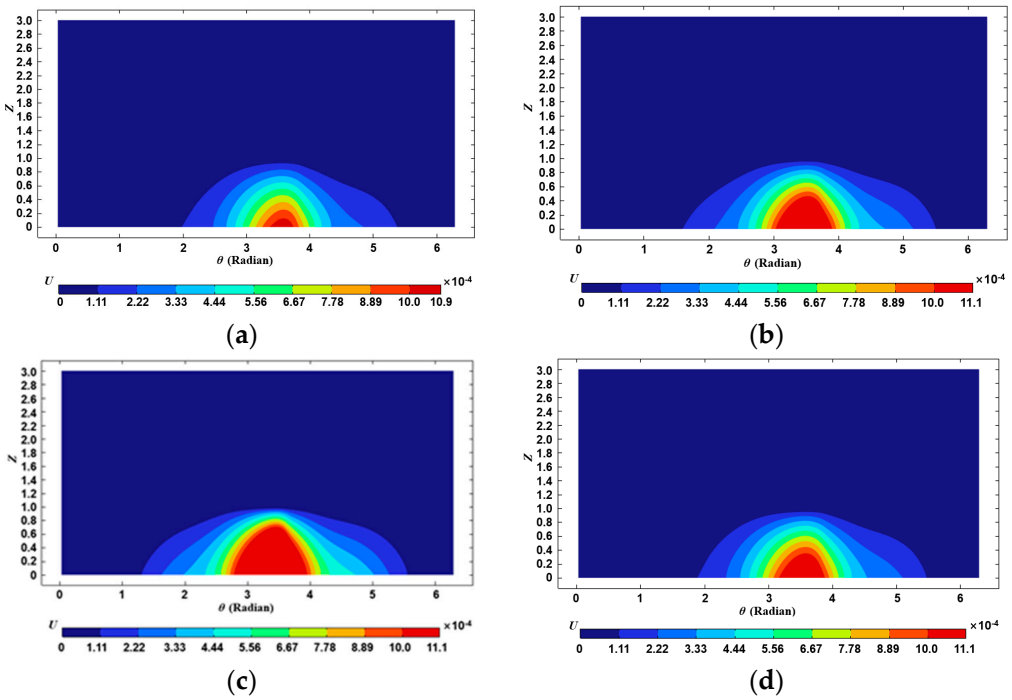

Figure 13. *Cont.*

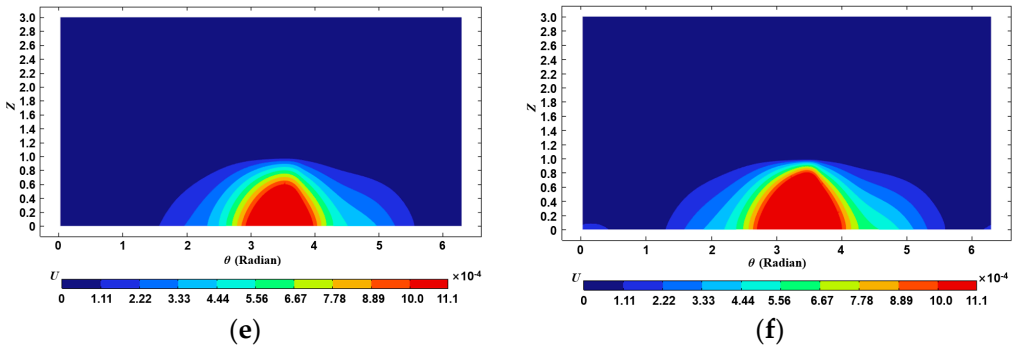

Figure 13. Dimensionless displacement distribution with E^* and W_{max}: (**a**) $E^* = 2.2 \times 10^4$, $W_{max} = 1.5\ W$; (**b**) $E^* = 2.2 \times 10^4$, $W_{max} = 2\ W$; (**c**) $E^* = 2.2 \times 10^4$, $W_{max} = 3\ W$; (**d**) $E^* = 1.5 \times 10^4$, $W_{max} = 1.5\ W$; (**e**) $E^* = 1.5 \times 10^4$, $W_{max} = 2\ W$; (**f**) $E^* = 1.5 \times 10^4$, $W_{max} = 3\ W$.

In this investigation, we performed changes in the dimensionless minimum film thickness in relation to variations in the dimensionless length (L_f) of the flexible structure, as shown in Figure 14. The lubrication characteristics were compared under three load conditions and two elastic modulus conditions with other specifications shown in Table 2. In a previous study [23], there was no metal-to-metal contact when L_f was 0.2 under the condition of a dimensionless static load, W. However, metal-to-metal contact occurred under the condition of an impact load being applied along with the static load. When L_f was 0.2, the flexible structure covered a very small area, 20% of the bearing's axial length. It is believed that it is difficult to secure a sufficient oil film due to deformation under conditions where impact load is also applied. Thus, numerical analysis was performed only for L_f between 0.3 and 0.6. Figure 14a,b show the results obtained for dimensionless elastic moduli of 2.2×10^4 and 1.5×10^4, respectively. When the dimensionless elastic modulus is reduced by about 32%, these changes in dimensionless minimum film thickness are expressed as a percentage, as shown in Figure 14b. This percentage quantifies the difference in dimensionless minimum film thickness between the two elastic moduli, based on the dimensionless minimum film thickness when the dimensionless elastic modulus is 2.2×10^4. When the dimensionless elastic modulus was 2.2×10^4, the variance in the dimensionless minimum film thickness was relatively small when the maximum load was 1.5 and 2 times the static load. However, when the maximum load was 3 times the static load, the difference in the dimensionless minimum film thickness became significantly smaller, as shown in Figure 14a. In Figure 14b, it can be seen that if the dimensionless elastic modulus was changed to a small value, the lubrication characteristics were improved in terms of minimum film thickness. In particular, when L_f was small, the improvement in the lubricating characteristics was greater due to changes in the dimensionless elastic modulus than when it was large. Moreover, when L_f increased under the same load condition, the percentage generally decreased. That is, when L_f increased and the elastic modulus decreased, the increase rate of the minimum film thickness was not large; thus, the improvement in the lubricating characteristics was not distinct.

Table 2. Specification of the analysis model (variation in L_f, W and E^*).

Parameter	Value	Parameter	Value
A	0.4	W	$W_{max} = 1.5\ W, 2\ W, 3\ W$
E^*	2.2×10^4, 1.5×10^4	β	10^{-3}
L	3.0	γ	1.0
L_f	0.3, 0.4, 0.5, 0.6	ε'	0.2
P_b	0.3		

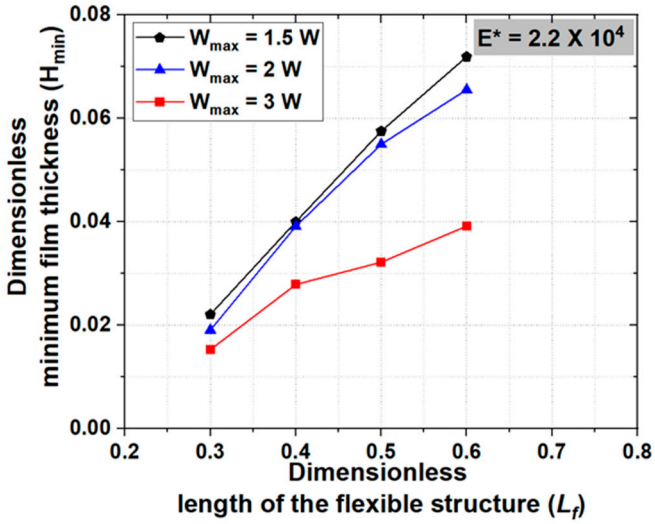

(**a**)

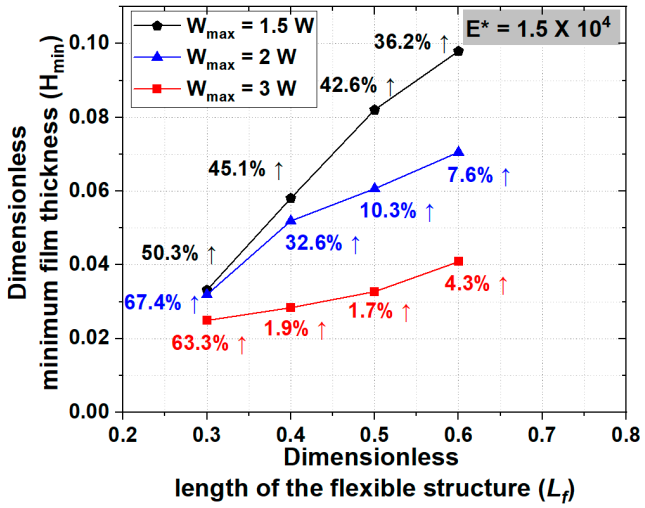

(**b**)

Figure 14. Dimensionless minimum film thickness with L_f and W_{max}: (**a**) $E^* = 2.2 \times 10^4$; (**b**) $E^* = 1.5 \times 10^4$.

Figure 15 illustrates the changes in the non-dimensional minimum film thickness with changes in the tilting ratio (ε'). Furthermore, we compared lubrication characteristics across three different load conditions and two elastic modulus conditions, with the specifications and details outlined in Table 3. When the dimensionless elastic modulus was 2.2×10^4 under the three load conditions, the non-dimensional minimum film thickness varied with changes in the tilting ratio, as shown in Figure 15a. As the tilting ratio was increased, the dimensionless minimum film thickness decreased. This was because as the tilting ratio was increased, misalignment became more severe, resulting in unstable driving conditions that made it difficult to secure a sufficient oil film. In previous studies [23] where a static load was applied, an oil film was secured and the lubrication characteristics were good, even at a tilting ratio of 0.4. However, under conditions where an impact load was also applied, metal-to-metal contact occurred when the tilting rate exceeded 0.2. Thus, we tried to change the dimensionless elastic modulus in order to improve the lubrication characteristics. When the dimensionless elastic modulus is reduced by about 32%, these variations in dimensionless minimum film thickness are expressed as a percentage, as shown in Figure 15b. These percentages were obtained in the same manner as previously mentioned. Due to change in the elastic modulus, the increase rate of the minimum oil

film thickness at the tilting rate was smaller than the increase rate of the minimum film thickness with the same dimensionless thickness and length of the flexible structure. If the tilting ratio was large, the increase rate of the dimensionless minimum film thickness was large upon changing the dimensionless elastic modulus. However, when the tilting ratio was small, the improvement upon changing the dimensionless elastic modulus was negligible. Overall, it was ineffective in terms of improving the lubrication characteristics by facilitating elastic deformation by reducing the non-dimensional elastic coefficient with the change in tilting rate.

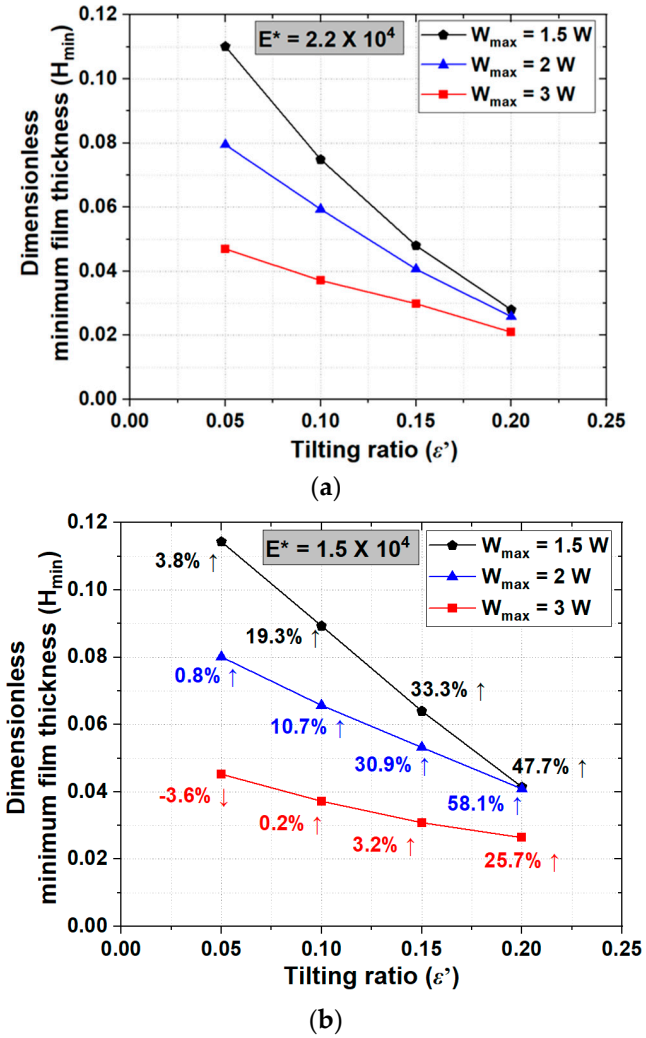

Figure 15. Dimensionless minimum film thickness with ε' and W_{max}: (**a**) $E^* = 2.2 \times 10^4$; (**b**) $E^* = 1.5 \times 10^4$.

Table 3. Specification of the analysis model (variation in ε').

Parameter	Value	Parameter	Value
A	0.4	W	W_{max} = 1.5 W, 2 W, 3 W
E^*	2.2×10^4, 1.5×10^4	β	10^{-3}
L	3.0	γ	1.0
L_f	1/3	ε'	0.05, 0.1, 0.15, 0.2
P_b	0.3		

4. Conclusions

This study demonstrates the utilization of a flexible structure in enhancing the lubrication performance of misaligned journal bearings under shock load conditions. Shock loads applied for various reasons can cause wear and failure due to contact in misaligned journal bearings. To improve this phenomenon, a flexible structure that could facilitate elastic deformation was applied to the end of the journal bearing, and EHL analysis was performed on misaligned journal bearings. The impact load of the journal bearing was assumed to be in the form of a wave. It was applied in addition to the static load. Three conditions were used, in which the overall maximum load was applied at 1.5, 2 and 3 times the static load. In addition, in order to improve the conditions of poor lubrication, such as metal-to-metal contact, the elastic modulus was reduced within the range of the elastic modulus of bearing steel currently used, and the lubrication characteristics were compared with those of the existing elastic modulus. The assessment of lubrication performance involved a comparison of the minimum film thickness of the journal bearing equipped with a flexible structure using different dimensionless thicknesses, lengths and tilting ratios. The dimensionless thickness ratio (γ) for the flexible structure remained constant at 1, since it was determined that the rectangular-shaped flexible structure outperformed the tapered one in terms of enhancing lubrication properties in previous research. The application of the flexible structure of misaligned journal bearings is very effective in improving lubrication characteristics under impact load conditions. This is because even if an impact load is added to the static load, a sufficient oil film thickness is secured due to elastic deformation in the flexible structure. A misaligned journal bearing with a flexible structure could prevent metal-to-metal contact until a maximum load of approximately three times the rated load is reached. When contact occurs or the lubrication performance is poor in a misaligned journal bearing with a flexible structure, the lubrication performance is significantly improved by changing the modulus of elasticity to be slightly lower. Finally, the numerical results showed that the application of a flexible structure to misaligned journal bearings improved the lubrication characteristics under impact load conditions. However, from an empirical perspective, additional research is needed to apply experimental verification to actual systems such as compressors and hydraulic pumps.

Author Contributions: Conceptualization, S.-H.H. and W.-J.J.; literature review and formal analysis, S.-H.H.; writing-original draft preparation, methodology, S.-H.H.; review and editing, S.-H.H.; funding acquisition, S.-H.H. All authors have read and agreed to the published version of the manuscript.

Funding: This work was supported by Korea Hydro & Nuclear Power Co. (2023).

Data Availability Statement: Not applicable.

Acknowledgments: This work was supported by a Korea Institute of Energy Technology Evaluation and Planning (KETEP) grant funded by the Korean government (MOTIE) (No. 20214000000010).

Conflicts of Interest: The authors declare no conflict of interest.

Nomenclature

A	Dimensionless thickness of the flexible structure (=a/r)
E	Modulus of elasticity (GPa)
E^*	Dimensionless modulus of elasticity (=$c^2E/(6r^2\eta\omega)$)
F	Dimensionless force (=$c^2f/(6r^4\eta\omega)$)
F_O	Dimensionless oil film force (=$c^2f_o/(6r^4\eta\omega)$)
F_X	Dimensionless force in the X direction
F_Y	Dimensionless force in the Y direction
F_Z	Dimensionless force in the Z direction
F_{OX}	Dimensionless oil film force in the X direction
F_{OY}	Dimensionless oil film force in the Y direction
H	Dimensionless oil film thickness (=h/c)

H_e	Dimensionless oil film thickness variation by elastic deformation (=h_e/c)
H_m	Dimensionless minimum film thickness (=h_m/c)
L	Ratio of length to radius of the bearing (=l/r)
L_f	Dimensionless length of the flexible structure (=l_f/l)
O	Center of the shaft at the middle of the bearing
O_1, O_2	Center of the shaft at both ends of the bearing
P	Dimensionless oil film pressure (=$c^2(p - p_a)/(6r^2\ \eta\omega)$)
P_b	Dimensionless pressure at the bearing ends and oil feeding groove (=$c^2(p_b - p_a)/(6r^2\eta\omega)$)
T	Dimensionless time (=ωt)
T_1, T_3	Time interval in which static load acts
T_2	Time interval in which static and impact loads acts together
U	Dimensionless displacement in the element (=u/r)
W	Dimensionless load acting on the shaft (=$c^2w/(6r^4\eta\omega)$)
X, Y, Z	Dimensionless rectangular coordinate system ($X = x/r$, $Y = y/r$, $Z = z/r$)
a	Thickness at the outer end of the flexible structure (mm)
c	Clearance (μm)
d	Thickness at the inner end of the flexible structure (mm)
e	Tilting amount of the shaft (μm)
e'	Tilting amount of the shaft (μm)
f	Force (N)
f_o	Oil film force (N)
f_x	Force in the x direction (N)
f_y	Force in the y direction (N)
f_z	Force in the z direction (N)
f_{ox}	Oil film force in the x direction (N)
f_{oy}	Oil film force in the y direction (N)
h	Film thickness (μm)
h_e	Change in film thickness due to elastic deformation (μm)
h_m	Minimum film thickness (μm)
l	Length of the bearing (mm)
l_f	Length of the flexible structure (mm)
p	Oil film pressure (MPa)
p_a	Atmospheric pressure (MPa)
p_b	Pressure at bearing ends and oil feeding groove (MPa)
r	Radius of the bearing (mm)
t	Time (seconds)
u	Displacement in the element (mm)
w	Load acting on the shaft (N)
x, y, z	Rectangular coordinate system (mm)
β	Ratio of clearance to bearing radius (=c/r)
ε	Eccentricity ratio (=e/c)
ε'	Tilting ratio (=e'/c)
γ	Ratio of thickness at both ends of the flexible structure (=d/a)
η	Absolute viscosity of the lubricant (Pa·s)
ν	Poisson's ratio
θ	Cylindrical coordinate (rad)
θ_w	Direction of the load in the cylindrical coordinate system (rad)
ω	Angular velocity (rad/s)

References

1. Zakharov, S.M. Hydodynamic lubrication research: Current situation and future prospects. *J. Frict. Wear* **2010**, *31*, 56–67. [CrossRef]
2. Huang, Q.; Yan, X. Impact factors on lubricant performance of stern bearing with misaligned angle induced by transverse vibration of shaft. *Ocean Eng.* **2020**, *216*, 108051. [CrossRef]
3. Cabrera, D.L.; Wolley, N.H.; Allanson, D.R.; Tridimas, Y.D. Film pressure distribution in water-lubricated rubber journal bearing. *IMechE* **2005**, *219*, 125–132. [CrossRef]
4. Wang, N.; Meng, Q.; Wang, P.; Geng, T.; Yuan, X. Experimental research on film pressure distribution of water-lubricated rubber bearing with multiaxial grooves. *J. Fluids Eng.* **2013**, *135*, 084501. [CrossRef]

5. Zhang, Z.S.; Dai, X.D.; Zhang, Z.N.; Xie, Y.B. Thermoelastohydrodynamic behavior of misaligned plain journal bearings. *Proc. Inst. Mech. Eng. Part C J. Mech. Eng. Sci.* **2013**, *227*, 2582–2599. [CrossRef]
6. Zheng, L.; Zhu, H.; Zhu, J.; Deng, Y. Effects of oil film thickness and viscosity on the performance of misaligned journal bearings with couple stress lubricants. *Tribol. Int.* **2020**, *146*, 106229. [CrossRef]
7. Das, S.; Guha, S.K.; Chattopadhyay, A.K. On the steady-state performance of misaligned hydrodynamic journal bearings lubricated with micropolar fluids. *Tribol. Int.* **2002**, *35*, 201–210. [CrossRef]
8. Liang, P.; Li, X.; Guo, F.; Cao, Y.; Zhang, X.; Jiang, F. Influence of sea wave shock on transient start-up performance of water-lubricated bearing. *Tribol. Int.* **2022**, *167*, 107332. [CrossRef]
9. Wang, C.; Zhang, C.; Gu, L.; Bi, M.; Hou, P.; Zheng, D.; Wang, L. Analysis on surface damage of M50 steel at impact-sliding contacts. *Tribol. Int.* **2020**, *150*, 106384. [CrossRef]
10. Wang, C.; Zang, C.; Bao, M.; Gu, L.; Wang, L.; Wei, X.; Li, W. Scratch damage on guiding surfaces of high-speed bearings under oil cut-off condition. *Eng. Fail. Anal.* **2022**, *140*, 106624. [CrossRef]
11. Xiang, G.; Han, Y.; Wang, J.; Xiao, K.; Li, J. A transient hydrodynamic lubrication comparative analysis for misaligned micro-grooved bearing considering axial reciprocating movement of shaft. *Tribol. Int.* **2019**, *132*, 11–23. [CrossRef]
12. Wang, Y.; Shi, X.; Zhang, I. Experimental and numerical study on water-lubricated rubber bearings. *Ind. Lubric. Tribol.* **2014**, *66*, 282–288. [CrossRef]
13. Murawski, L. Shaft line alignment analysis taking ship construction flexibility and deformations into consideration. *Mar. Struct.* **2005**, *18*, 62–84. [CrossRef]
14. Bouyer, J.; Fillon, M. An experimental analysis of misalignment effects on hydrohynamic plain journal bearing performances. *J. Tribol.* **2002**, *124*, 313–319. [CrossRef]
15. Sun, J.; Changlin, G. Hydrodyamic lubrication analysis of journal bearing considering misalignment caused by shaft deformation. *Tribol. Int.* **2004**, *37*, 841–848. [CrossRef]
16. Sun, J.; Gui, C.; Li, Z.; Li, Z. Influence of journal misalignment caused by shaft deformation under rotational load on performance of journal bearing. *Proc. Inst. Mech. Eng. Part J J. Eng.* **2005**, *219*, 275–283. [CrossRef]
17. Sun, J.; Gui, C.; Li, Z. An experimental study of journal bearing lubrication effected by journal misalignment as a result of shaft deformation under load. *J. Tribol.* **2005**, *127*, 813–819. [CrossRef]
18. Li, Q.; Liu, S.I.; Pan, X.H.; Zheng, S.Y. A new method for the studying the 3D transient flow of misaligned journal bearings in flexible rotor-bearing systems. *J. Zhejiang Univ. Sci. A* **2012**, *13*, 647–664. [CrossRef]
19. Pierre, I.; Bouyer, J.; Fillon, M. Thermohydrodynamic behavior of misaligned plain journal bearings: Theoretical and experimental approaches. *Tribol. Trans.* **2004**, *47*, 594–604. [CrossRef]
20. Xu, G.; Zhou, J.; Geng, H.; Lu, M.; Yang, I.; Yu, L. Research on the static and dynamic characteristics of misaligned journal bearing considering the turbulent and thermohydrodynamic effects. *J. Tribol.* **2015**, *137*, 024504. [CrossRef]
21. Li, B.; Sun, J.; Zhu, S.; Fu, Y.; Zhao, X.; Wang, H.; Teng, Q.; Ren, Y.; Li, Y.; Zhu, G. Thermohydrodynamic lubrication analysis of misaligned journal bearing considering the axial movement of journal. *Tribol. Int.* **2019**, *135*, 397–407. [CrossRef]
22. Nikolakopoulos, P.G.; Papadopoulos, C.; Kaiktsis, I. Elastohydrodynamic analysis and Pareto optimization of intact, worn and misaligned journal bearings. *Meccanica* **2011**, *46*, 577–588. [CrossRef]
23. Jeon, W.J.; Hong, S.H. A new type of misaligned journal bearing with flexible structure. *Lubricants* **2023**, *11*, 256. [CrossRef]
24. Thomsen, K.; Klit, P. Improvement of journal bearing operation at heavy misalignment using bearing flexibility and compliant liners. *Proc. Inst. Mech. Eng. Part J J. Eng. Tribol.* **2012**, *226*, 651–660. [CrossRef]
25. Sharma, S.C.; Girish, B.M.; Kamath, R.; Satish, B.M. Graphite particles reinforced ZA-27 alloy composite materials for journal applications. *Wear* **1998**, *219*, 162–168. [CrossRef]
26. Kim, S.S.; Park, D.C.; Lee, D.G. Characteristics of carbon fiber phenolic composite for journal bearing materials. *Compos. Struct.* **2004**, *66*, 359–366. [CrossRef]
27. Bouyer, J.; Fillon, M. Improvement of the THD performance of a misaligned plain journal bearing. *J. Tribol.* **2003**, *125*, 334–342. [CrossRef]
28. Hattori, H. EHL analysis of a journal bearing for rotary compressors under dynamic loading: Effect of flexible structure at bearing end. *Trans. Jap. Soc. Mech. Eng.* **1998**, *64*, 3171–3178. [CrossRef]
29. Ito, Y.; Hattori, H.; Miura, K. Mixed lubrication analysis of vane sliding surface in rotary compressor mechanisms. *Tribol. Online* **2009**, *4*, 96–102. [CrossRef]
30. Ikeda, A.; Satodate, K.; Aoki, T.; Miura, K. Development of the rotary compressor which is high performance in the wide range, and has high refrigerating capacity. In Proceedings of the JSRAE Annual Conference, Tokyo, Japan, 12–14 September 2012.
31. Tao, Y.; Zhao, J.; Feng, S.Z. A reliability assessment model for journal bearing based on natural degradation and random shocks. *J. Mech. Sci. Technol.* **2020**, *34*, 4641–4648. [CrossRef]
32. Lee, J.; Jang, G.; Jung, K. Optimal design of fluid dynamic bearings to develop a robust disk-spindle system in a hard disk drive utilizing model analysis. *Microsyst. Technol.* **2013**, *19*, 1495–1504. [CrossRef]
33. Jang, G.H.; Yoon, J.W. Nonlinear dynamic analysis of a hydrodynamic journal bearing considering the effect of a rotating or stationary herringbone groove. *J. Tribol.* **2002**, *124*, 297–304. [CrossRef]
34. Park, K.Y.; Jang, G.H. Dynamic of a hard disk drive spindle system due to its structural design variables and the design variables of fluid dynamic bearings. *IEEE Trans. Magn.* **2009**, *45*, 5135–5140. [CrossRef]

35. Walton, J.F.; Heshmat, H.; Tomaszewski, M.J. Testing of s small turbocharger/turbojet sized simulator rotor supported on foil bearings. *J. Eng. Gas Turbines Power* **2004**, *130*, 67–73. [CrossRef]
36. Zhang, Q.D.; Shan, X.C. Dynamic characteristics of micro air bearings for microsystems. *Microsyst. Technol.* **2008**, *14*, 229–234. [CrossRef]
37. Ren, T.M.; Feng, M. Anti-shock characterictics of water lubricated bearing for fuel cell vehicle air compressor. *Tribol. Int.* **2017**, *107*, 56–64. [CrossRef]
38. Jamali, H.U.; Sultan, H.S.; Abdullah, O.I.; Al-Tamimi, A.N.J.; Abbud, L.H.; Ruggiero, A.; Al-Dujaili, Z.A. Effect of chamfer form and parameters on the characteristics of finite length journal bearing under impact load. *Lubricants* **2023**, *11*, 73. [CrossRef]
39. Jamali, H.U.; Sultan, H.S.; Abdullah, O.I.; Al-Tamimi, A.N.J.; Abbud, L.H.; Ruggiero, A.; Al-Dujaili, Z.A. Analysis of the performance of chamfered finite-length journal bearings under dynamic loads. *Mathematics* **2023**, *11*, 587. [CrossRef]
40. Pai, R.; Majumdar, B.C. Stability of submerged four-lobe oil journal bearings under dynamic load. *Wear* **1992**, *154*, 95–108. [CrossRef]
41. Strzelecki, S. Operating characteristics of heavy loaded cylindrical journal bearing with variable axial profile. *Mater. Res.* **2005**, *8*, 481–486. [CrossRef]
42. Nacy, S.M. Effect of chamfering on side-leakage flow rate of journal bearings. *Wear* **1997**, *212*, 95–102. [CrossRef]
43. Nicoletti, R. Optimization of journal bearing profile for higher dynamic stability limits. *J. Tribol.* **2012**, *135*, 011702. [CrossRef]
44. Ghosh, M.K.; Satish, M.R. Stability of multillobe hybrid bearing with short sills—Part II. *Tribol. Int.* **2003**, *36*, 633–636. [CrossRef]
45. Jiang, L.; Feng, Q.; Coit, D.W. Modeling zoned shock effects on the stochastic degradation in dependent failure processes. *IIE Trans.* **2015**, *47*, 460–470. [CrossRef]
46. Song, S.I.; Coit, D.W.; Feng, Q.M. Reliability analysis of multi-component series systems subject to hard and soft failures with dependent shock effects. *IIE Trans.* **2016**, *48*, 720–735. [CrossRef]
47. Hong, S.H.; Kim, K.W. A new type groove for hydraulic spool valve. *Tribol. Int.* **2016**, *103*, 629–640. [CrossRef]
48. Oh, K.P.; Huebner, K.H. Solution of the elastohydrodynamic finite journal bearing problem. *ASME Lubr. Technol.* **1973**, *95*, 342–351. [CrossRef]
49. Kalin, M.; Kus, M. New strategy for reducing the EHL friction in steel contacts using additive-formed oleophobic boundary film. *Friction* **2021**, *9*, 1346–1360. [CrossRef]
50. Wang, Y.; Wang, Q.J.; Lin, C. A mixed-EHL analysis of effects of misalignments and elastic deformations on the performance of a coupled journal-thrust bearing system. *Tribol. Int.* **2006**, *39*, 281–289. [CrossRef]
51. Cai, J.; Xiang, G.; Li, S.; Guo, J.; Wang, J.; Chen, S.; Yang, T. Mathematical modeling for nonlinear dynamic mixed friction behaviorsof novel coupled bearing lubricated with low viscosity fluid. *Phys. Fluids* **2022**, *34*, 093612. [CrossRef]
52. Zhou, Y.; Wang, Y.; Zhao, J. Influence on journal bearing considering wall-slip in EHL. *IOP Conf. Ser. Mater.* **2018**, *394*, 042042. [CrossRef]
53. Xiang, G.; Yang, T.; Guo, J.; Wang, J.; Liu, B.; Chen, S. Optimization transient wear and contact performances of water-lubricated bearings under fluid-solid-thermal coupling condition using profile modification. *Wear* **2022**, *502–503*, 204379. [CrossRef]